SCIENTIFIC REPORTS

OPEN

SUBJECT AREAS:
ELECTROCHEMISTRY
MATERIALS FOR ENERGY AND CATALYSIS

Received
12 December 2013

Accepted
3 March 2014

Published
9 May 2014

Correspondence and requests for materials should be addressed to M.V.S. (mv.shelke@ncl.res.in; shelkemanju@gmail.com)

C@SiNW/TiO_2 Core-Shell Nanoarrays with Sandwiched Carbon Passivation Layer as High Efficiency Photoelectrode for Water Splitting

Rami Reddy Devarapalli[1,2], Joyashish Debgupta[1], Vijayamohanan K. Pillai[1,2,3,4] & Manjusha V. Shelke[1,2,3]

[1]Physical and Materials Chemistry Division, CSIR-National Chemical Laboratory (CSIR-NCL), Pune- 411 008, MH, India, [2]Academy of Scientific and Innovative Research (AcSIR), Anusandhan Bhawan, 2 Rafi Marg, New Delhi-110 001, India, [3]CSIR-Network Institute for Solar Energy, CSIR-National Chemical Laboratory, Pune-411008, MH, India, [4]CSIR-Central Electro Chemical Research Institute, Karaikudi-630006, Tamilnadu, India.

One-dimensional heterostructure nanoarrays are efficiently promising as high performance electrodes for photo electrochemical (PEC) water splitting applications, wherein it is highly desirable for the electrode to have a broad light absorption, efficient charge separation and redox properties as well as defect free surface with high area suitable for fast interfacial charge transfer. We present highly active and unique photoelectrode for solar H_2 production, consisting of silicon nanowires (SiNWs)/TiO_2 core-shell structures. SiNWs are passivated to reduce defect sites and protected against oxidation in air or water by forming very thin carbon layer sandwiched between SiNW and TiO_2 surfaces. This carbon layer decreases recombination rates and also enhances the interfacial charge transfer between the silicon and TiO_2. A systematic investigation of the role of SiNW length and TiO_2 thickness on photocurrent reveals enhanced photocurrent density up to 5.97 mA/cm^2 at 1.0 V vs.NHE by using C@SiNW/TiO_2 nanoarrays with photo electrochemical efficiency of 1.17%.

Unprecedented rise in global energy-demands concomitant to rapid decrease in fossil fuel sources and growing concerns over changing climate situations have provoked development of new technologies to harness energy from clean and renewable sources. Hydrogen is widely regarded as one of the most likely chemical energy sources that can offer viable solutions to resolve many current energy issues. Mass production of hydrogen by an economically competitive and environmentally beneficial technique is essential for generalized acceptance of hydrogen as universal fuel. Photo electrochemical (PEC) splitting of water by using solar energy is one of the most promising processes for the utilization of the solar energy to generate hydrogen[1–5]. However, many material challenges associated with the development of efficient photo electrodes for practical PEC applications need pragmatic solutions in order to obtain high photocurrent density with a broad spectrum of absorption, matching energy band levels to water reduction/oxidation energy levels along with high stability in aqueous environment. One dimensional (1D) semiconducting nanomaterials are looked upon as efficient photo electrode materials for PEC water splitting because of their inherent features like 1D electron transport, enhanced charge collection efficiency, less reflectivity and larger interfacial area with the electrolyte[6–11]. Since the first demonstration of water splitting with TiO_2[12], aggressive research efforts are going on to synthesize 1D nanostructures of various semiconducting materials like ZnO, WO_3, SnO_2, Cu_2O, CdSe, CdS, CdTe, PbS, Si, Fe_2O_3, GaP in order to significantly improve the efficiency of water splitting reaction[13–23]. Si based photo electrodes have obvious advantages over other semiconducting materials with a band gap of 1.12 eV which allows light absorption over broad range of solar spectrum and also possess higher conductivity that facilitates efficient charge collection[24–26]. In addition, Si is the most abundant material on earth and has already demonstrated its importance in photovoltaic devices[24,27]. For example, in some recent studies, P-type or n-type Si nanowire (SiNW) arrays have shown improved PEC properties as photocathode or a photo anode, respectively[28]. However, effective use of silicon as a photoelectrode material for PEC is limited by the facts that it easily gets oxidized in water and its valence band energy is higher than that of the water oxidation energy level. Minimizing these limitations and exploiting excellent optical and electronic properties of Si for PEC devices should be possible by making hybrid

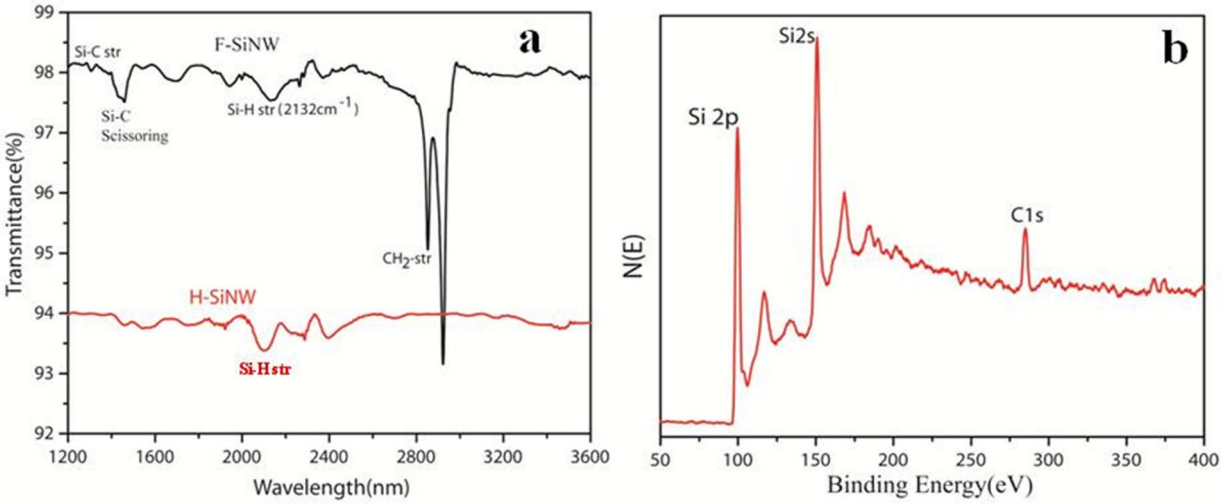

Figure 1 | (a) A comparison of the FT-IR spectra of H-SiNWs and Alkyl functionalized SiNWs respectively and (b) XPS spectra of the carbon passivated SiNWs.

heterojunction nanomaterials of silicon with another complementary materials in a way that each semiconductor will satisfy one energetic requirement i.e. matching conduction band minimum (CBM) or valence band maximum (VBM) with either O_2 oxidation or H_2 reduction potential[29]. In this regard core shell heterostructures of Si with various semiconductors like TiO_2, ZnO, Fe_2O_3 and InGaN have recently emerged as new building blocks for efficient PEC devices[30–34]. The large oxidizing power of photo generated holes in TiO_2 and sustained chemical stability makes them perhaps as ideal candidate of choice for heterojunction formation with Si[35]. In a recent report, three dimensional hierarchical TiO_2 nanostructures have been prepared on SiNWs by atomic layer deposition (ALD) to increase the effective electrode surface area and enhanced photocurrent densities upto 3.64 mA/cm^2 are achieved[29]. However, nothing is mentioned on stability. For the preparation of silicon based nano heterojunction, SiNWs have been synthesized by various techniques like metal assisted chemical etching (MacEtch), deep reactive etching (DRIE), vapour-liquid-solid (VLS) technique, Laser-assisted growth, and molecular beam epitaxial (MBE). Interestingly, Nanowires synthesized by MacEtch show enhanced solar energy conversion efficiency by two orders of magnitude higher than that for SiNWs prepared by other methods perhaps because of vertical alignment to improve light absorption significantly[36]. However, SiNWs prepared by this technique possess lot of defects on its surface which act as recombination sites for electron-hole pairs and reduce the minority carrier diffusion life time. Surface passivation of SiNWs obviates these limitations by reducing these defect sites subsequently to decrease the recombination rates and to improve the water splitting efficiency considerably. This passivation layer also prohibits the formation of SiO_2 layer in water during the reaction or while coating other material on SiNWs. So far most of the research is focused on coating a protective layer on Si electrode surface by using techniques like ALD; Plasma enhanced chemical vapour deposition (PECVD), and Metal organic chemical vapour deposition (MOCVD). Similar techniques are used for heterojunction formation as well; however, these are extremely critical, expensive processes. One needs to develop cost effective, solution processable technique to passivate surface of SiNWs and/or to fabricate nano-heterojunction with other size-tuneable semiconductors without too many experimental difficulties.

In this paper, we report an innovative approach of chemically functionalizing SiNWs surface by photochemical alkylation of hydrogen terminated SiNWs. Subsequently to convert it into ultrathin passivation layer of carbon by annealing at high temperature in an inert atmosphere followed by dip coating of TiO_2 thin layer in order to fabricate surface passivated Silicon-TiO_2 core shell nanowire arrays. These core shell nanowire arrays with thin sandwiched carbon passivation layer are used as photo anode for electrochemical water splitting to achieve superior enhancement in the photo electrochemical properties. The Passivation layer of carbon does several remarkable functions at the same time such as reducing the defect sites, decreasing the recombination rates and finally also enhancing the interfacial charge transfer between the silicon and TiO_2 effectively to facilitate device fabrication.

Results

SiNW arrays prepared by MacEtch process are prone to get oxidized in air and aqueous environments to form a layer of SiO_2 on its surface. Hence a protective layer is essentially required to control this oxidation during water splitting experiments. In order to make an ultrathin passivation layer, wet etched H-terminated SiNWs functionalized by photochemical alkylation. H-terminated SiNWs were reacted with 1-octene under controlled atmosphere and UV irradiation. The photochemical reaction occurs between Si-H and C=C bond and forms Si-C bond via a radical mechanism[37]. Figure 1(a) shows a comparison of the FT-IR spectra of H-SiNWs and alkyl functionalized SiNWs (F-SiNWs) respectively. In case of H-SiNWs, peaks are observed for stretching mode $\nu_{Si\text{-}Hx}$ centred at 2132 cm^{-1}. After photochemical alkylation reaction with 1-octene molecule, H-SiNWs are converted to the alkyl functionalized SiNWs and consequently the FT-IR spectrum shows methylene (CH_2) antisymmetric and symmetric stretching characteristic peaks at 2923 cm^{-1} and 2852 cm^{-1} and Si-C bending peak at 1458 cm^{-1} confirming the alkyl groups. Alkylated SiNW array substrate was then annealed in an argon atmosphere at 500°C for two hours. Organic molecules present on SiNWs surface were converted into ultra-thin carbon layer that passivated the surface of SiNWs by reducing defects; it also acts as protective layer preventing SiO_2 formation in aqueous medium. More importantly, this thin carbon layer decreases the recombination rates and also enhances the interfacial charge transfer between silicon and TiO_2 by tunnelling. The formation of carbon on the SiNWs is confirmed by X-ray photoelectron spectroscopy (XPS). Figure 1(b) shows a typical broad-scan XP spectrum of the surface passivated SiNWs. The intense signals at 99 eV and 148 eV binding energy correspond to the silicon 2 p and 2 s electrons respectively. The signal at 284 eV corresponds to the C 1 s electron, which could be considered as an evidence for the formation of carbon after annealing of alkyl groups on the SiNWs.

The formation of the carbon layer from the alkyl groups is also confirmed by the water contact angle measurements, which are shown in the supporting information S1. Figure 2 displays distinct SEM images of the SiNWs and Si/TiO_2 core shell nanoarrays both before and after surface passivation with the carbon (C@SiNWs), using TiO_2 layer on it by dip coating. More specifically, Figure 2(a, b) shows top and tilted views of SEM images of C@SiNWs while Figure 2(c, d) shows similar top and tilted views of TiO_2 coated C@SiNWs. Length of these nanowires is approximately 6 μm and thickness of TiO_2 shell is around 30 nm which are very crucial for their enhanced performance. The formation of TiO_2 on SiNWs was further confirmed by X-ray diffraction (XRD) (Supporting information, Figure S2) where coated TiO_2 exists in tetragonal anatase phase with diffraction peaks at 2θ values of 25.3°, 47.9°, 54.6° and 56.3° corresponding to (101), (200), (211) and (105) planes respectively with lattice parameters comparable to that in the reported data (JCPDS card no:01-086-1155). Further the diffraction peak at 31.3° corresponds to the Si (200) plane.

Figure 3(a) displays the TEM image of C@SiNWs/TiO_2 nanowires while 3(b) reveals the corresponding HRTEM image of Si/TiO_2 interfacial region. More significantly, the d-spacing of TiO_2 on the top of the silicon is 0.356 nm [Figure 3(c)], which resembles the d-spacing value of the TiO_2 (101) plane from XRD. Figure 3(d) shows SAED of Si/TiO_2 interfacial region showing silicon (200) and TiO_2 (101) planes in the diffraction pattern. Reflectance measurements of the samples including plane Si wafer, C@Si, C@Si/TiO_2, C@SiNW and C@SiNWs/TiO_2 are carried out (supporting information Figure S3) in order to prove that the thin passivation carbon layer does not adversely affect the optical absorption properties of silicon. Although after coating the TiO_2 layer on carbon passivated silicon wafer, more than 10% decrease in the reflectance occurs obviously due to the antireflective behaviour of TiO_2, C@SiNWs and C@SiNWs/TiO_2 samples show less overall reflectance particularly in the UV-Vis region (less than 5%). Due to the antireflective properties of the TiO_2, there is no change in the optical absorption of the C@SiNWs thus facilitating maximum absorption of solar energy. The photo electrochemical properties of these heterostructure nanoarrays have been analyzed by using them as photo electrode for PEC water splitting cells in 1 M KOH electrolyte by linear sweep voltammetry. Typical plots of photocurrent density versus bias potential of SiNW/TiO_2 and C@SiNWs/TiO_2 nanoarrays (length 6 μm, thickness of TiO_2 layer 30 nm) under dark and simulated solar light illumination conditions are shown in Figure 4. Although the dark current density of the samples remain at relatively low level (less than 0.5 mA/cm^2) under bias potentials between −1 to 1 V (vs. NHE), higher photocurrent density of 5.97 mA/cm^2 at 1.0 V vs. NHE is evident by using C@SiNWs/TiO_2 arrays, while unpassivated SiNW/TiO_2 nanowire arrays reveal only a photo current density of 3.67 mA/cm^2 at the same bias. In comparison, Surface passivated C@SiNWs/TiO_2 nanoarrays show 61% more photocurrent density than that of the unpassivated SiNWs/TiO_2 samples at 1.0 V vs. NHE bias potential. The change in the onset potentials between the SiNW/TiO_2 photoelectrodes with and without surface passivation of SiNWs is also significantly noticeable. For example, C@SiNWs/TiO_2 photo electrode shows an onset potential at −0.88 V vs. NHE, whereas SiNWs/TiO_2 photoelectrode shows only −0.55 V vs.NHE. The importance of surface passivation layer on SiNWs in SiNW/TiO_2 core-shell photoelectrodes is eminently displayed by these changes in the cathodic shift of onset potentials around 330 mV and the photocurrent densities of the electrodes. This enhancement in the photocurrent of C@SiNWs/TiO_2 nanoarray photo electrode is mostly due to the surface passivation of SiNWs that decreases the defect distribution on its surface and thereby reduces the electron-hole recombination rates, ostensibly resulting in higher photocurrent density.

Discussion

In order to examine the effect of the surface passivation of silicon nanowires on the photocurrent densities, incident photon to current conversion efficiency (IPCE) test is extremely useful on C@SiNWs/TiO_2 nanoarray photoelectrodes. Accordingly, Figure 5(a) shows a comparison of the IPCE spectra of passivated and non passivated Si/TiO_2 and SiNW/TiO_2 photoelectrodes at an applied potential of 1.0 V vs. NHE. The photo electrodes prepared by plain silicon wafers

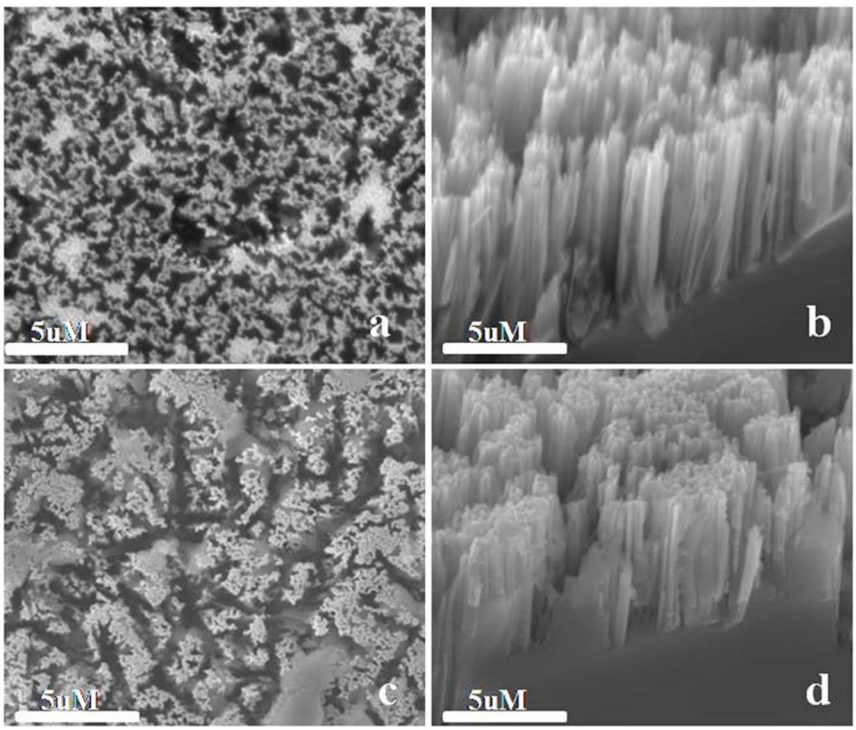

Figure 2 | Top and Tilted view of the SEM images of (a), (b) C@SiNWs and (c), (d) C@SiNW/TiO_2 core-shell nanoarrays.

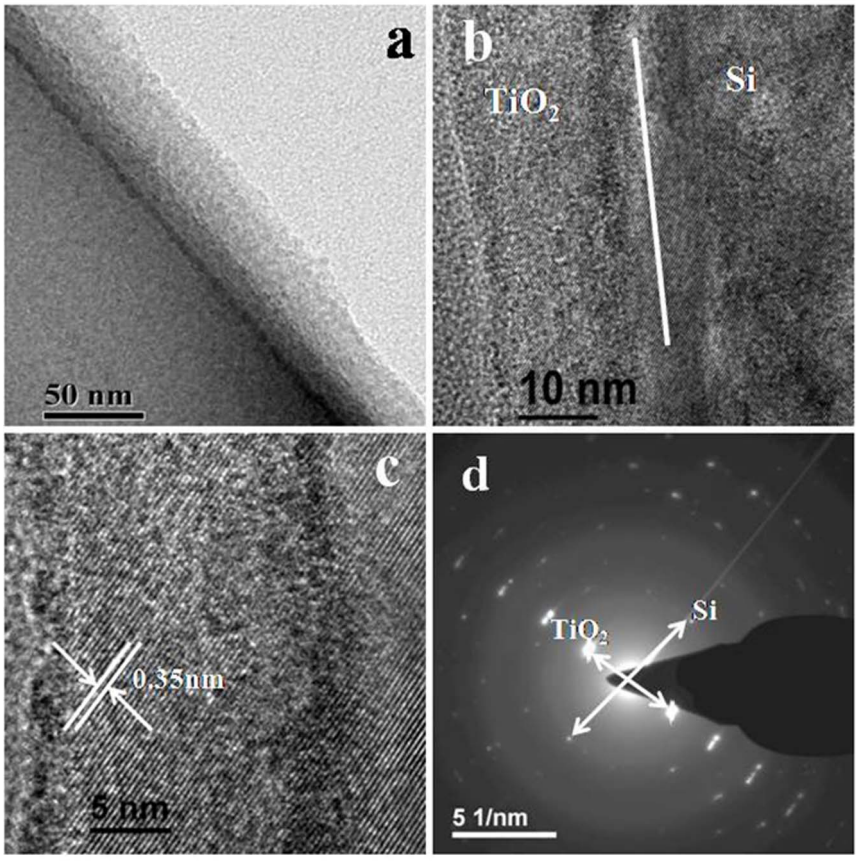

Figure 3 | **(a) TEM image, (b), (c) HRTEM images and (d) SAED pattern of C@SiNWs/TiO_2 core shell nanoarrays.**

show less IPCE values (less than 5%) compared to the photo electrodes prepared by using SiNWs. For instance, IPCE spectra of the SiNW/TiO_2 based photo electrodes show maximum photon to current conversion efficiencies in the visible and the near IR region, where SiNW absorbs more from the solar spectrum. More than 10% enhancement in the photon conversion efficiencies is observed between the SiNW/TiO_2 photo electrodes with and without surface passivation of SiNWs. Increase in the IPCE values after surface passivation of SiNWs is perhaps due to decrease in defect sites on the surface of SiNWs; otherwise these defects are the potential cause for recombination of electron-holes generated in the silicon by the absorption of light. Electrochemical impedance spectroscopy (EIS) is a useful tool to investigate the charge transport properties in this regard. The Nyquist plots of the obtained EIS data measured under the simulated solar light illumination are shown in Figure 5(b). The internal impedances are obtained by fitting the Nyquist plots to an equivalent circuit, which consists of an ohmic resistance and two RC elements in series, which account for the semiconductor and surface process respectively. Due to the fast charge transfer inside the bulk than the semiconductor electrolyte interface, high frequency response is assigned to the electronic process in the semiconductor with a resistance (R1) together with the constant phase element 1 (CPE1) whereas low frequency response is assigned to the semiconductor electrolyte interfacial charge transfer resistance (R2) along with constant phase element 2 (CPE2). The fitted equivalent circuit is shown in the inset of figure 5b and the fitted results are summarized in table 1.The values of R2 and corresponding values of CPE2 for C@SiNWs/TiO_2 and SiNWs/TiO_2 are 23,907 ohm, 56,223 ohm, 7.39×10^{-6} F and 21.59×10^{-6} F respectively. R2 corresponds to the interfacial charge transfer resistance between photo anode and the electrolyte and confirms that the passivation of SiNWs in C@SiNWs/TiO_2 nanoarray photoelectrodes increases charge transfer rate between the electrode and the electrolyte. The parameters in Table 1 can be explained by the fact that a decrease in defect sites in SiNWs by passivation layer leads to less recombination of photo generated excited electrons with the holes in silicon. Then the holes in the silicon recombine with the photo induced excited electrons generated in the TiO_2 layer easily. The holes present in the TiO_2 transfer into the electrolyte easily for oxidation reaction. In Addition, the presence of carbon between the Silicon and the TiO_2 enables fast charge transfer between the silicon and TiO_2. Whereas in case of unpassivated photo electrodes, recombination of photo

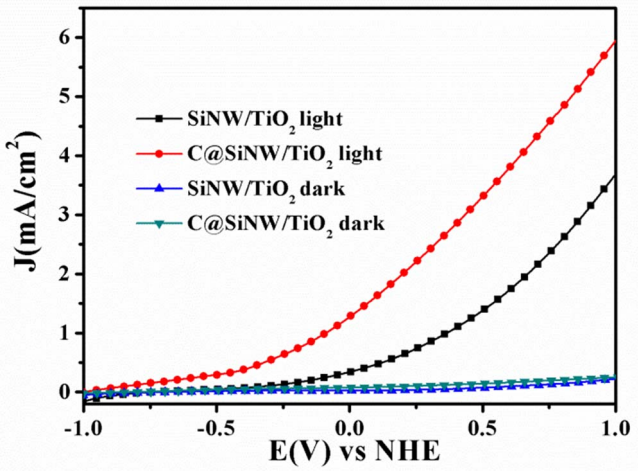

Figure 4 | **Photo electrochemical J-E curves under dark and illumination conditions for SiNWs/TiO_2 and C@SiNWs/TiO_2 nanoarrays (Height of SiNWs ~6 μm, TiO_2 layer thickness is 30 nm).**

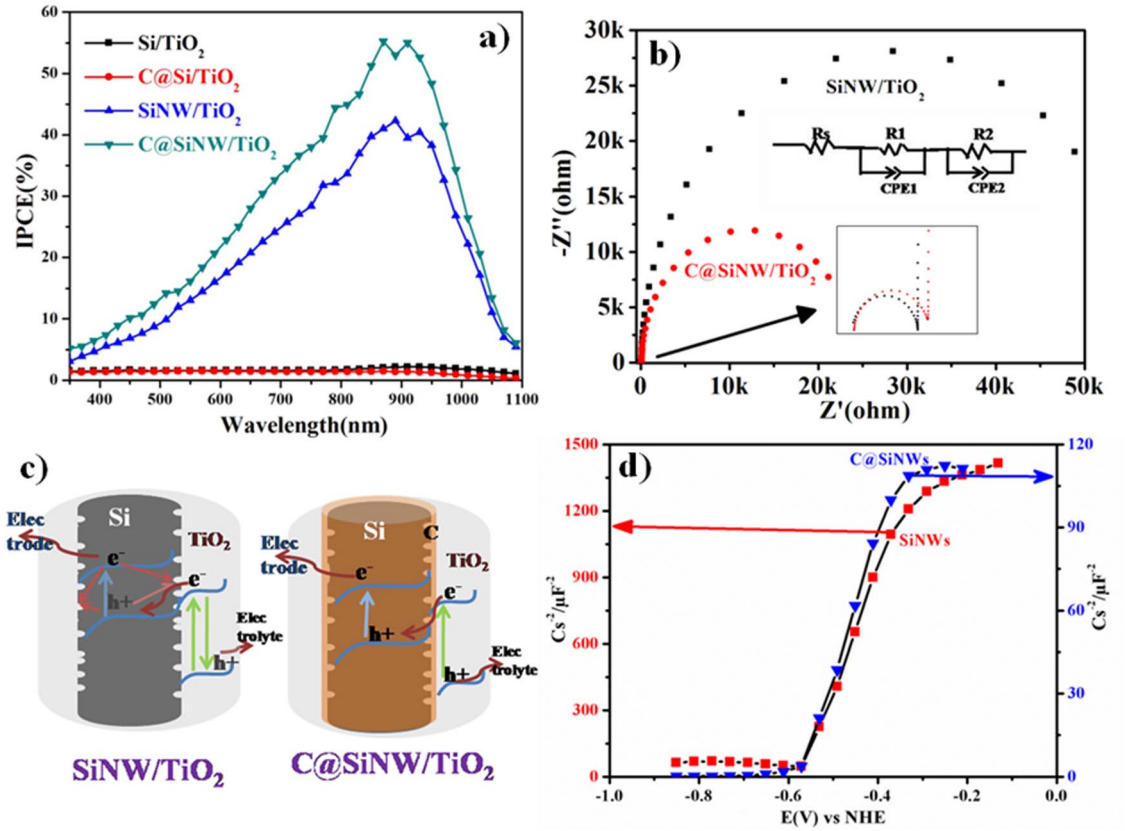

Figure 5 | (a) IPCE spectra of Si/TiO_2 and $C@Si/TiO_2$ wafer electrodes as well as $SiNWs/TiO_2$ and $C@SiNWs/TiO_2$nanoarray electrodes. (b) Nyquist plots of $SiNWs/TiO_2$ and $C@SiNWs/TiO_2$ core-shell nanowires under simulated solar light illumination. (c) Proposed electron transfer mechanism in $SiNW/TiO_2$ and $C@SiNW/TiO_2$ core-shell nanowire arrays (d). Mott-Schottky plots of SiNWs and C@SiNWs measured at 5 kHz.

generated electrons with holes at the defect sites in silicon is imminent thereby decreasing the charge transfer from the photo anode to the electrolyte. The minor negligible increment in the Rs and R1 values after passivation could be considered as an experimental error. The band level alignment and the electron transfer mechanism between SiNW and TiO_2 with and without carbon layer are illustrated in Figure 5(c). In order to verify the effect of carbon passivation on charge transport, the surface electronic properties like flat band potential and donor density of the surface passivated and unpassivated SiNWs are calculated by using the Mott-schottky plots. Mott-schottky analysis for SiNWs and C@SiNWs at a frequency of 5 kHz in 1 M KOH solution plots are shown in Figure 5(d). The flat band potential and the donor density are calculated by using the Mott-schottky equation

$$\frac{1}{C^2} = \frac{2}{\varepsilon\, \varepsilon o A^2 e N d}\left(V - Vfb - \frac{kBT}{e}\right) \qquad (1)$$

Where C is the specific capacitance (F/cm^2), e is the electron charge, ε the dielectric constant of Silicon (11.9), ε_0 the permittivity of vacuum, N_d the donor density, V the electrode applied potential, V_{fb} the flat-band potential, and k_BT/e has usual significance. By extrapolating the X-intercepts of the linear region in Mott−Schottky plots ($1/C^2$ vs. V), V_{fb} of SiNWs and C@SiNWs are found to be −0.58 and −0.59 V vs NHE respectively. There is no significant change in the V_{fb} after the surface passivation and a small change (10 mV) towards the negative side is expected for the surface state passivation[38]. From the observation of flat band potential values, it is confirmed that the carbon passivation layer does not change the properties of silicon except perhaps passivating the defects of the silicon nanowire surface. The donor densities (N_d) calculated from the mott-schottky equations for the SiNWs and C@SiNWs are $6.14*10^{15}$ and $14.9*10^{16}$ respectively. The increase of donor density after surface passivation suggests higher carrier generation and lower recombination losses at the surface of C@SiNWs than the unpassivated SiNWs. In order to estimate the role of TiO_2 on the enhancement of the photocurrent, photo electrochemical properties of the as prepared heterostructure arrays are analyzed by illuminating under only UV light and the typical current density and bias potential plots are shown in Figure S4 (supplementary information). Interestingly, $C@SiNW/TiO_2$ nanowires show higher photocurrent density than that of $SiNW/TiO_2$ nanowires under UV-light. This implies that the photocurrent density increases after the surface passivation of SiNWs and this increase in photocurrent of $C@SiNW/TiO_2$ than that on $SiNW@TiO_2$ electrodes is due to the less recombination losses at the interface between the Silicon and TiO_2.The dependence of photocurrent densities on thickness of the TiO_2 shell is also studied. Accordingly, Figure 6(a–c) shows the TEM images of $C@SiNWs/TiO_2$ nanowires with different thicknesses of TiO_2.While thickness of TiO_2 is varied, length of SiNWs is kept constant as 6 μm under similar surface passivation conditions. As TiO_2 sol is deposited by dip coating, coating cycles are optimized in order to achieve TiO_2 shell of varying thickness. The thicknesses of 10 ± 1 nm, 30 ± 1 nm and 50 ± 1 nm of TiO_2 on SiNWs prepared by dipping SiNWs substrate in sol solution for 10, 25 and 50 number of times respectively show consistent changes in

Table 1 | Electrochemical parameters determined from EIS analysis

System	Rs(Ω)	R1(Ω)	CPE1 (nF)	R2(Ω)	CPE2 (μF)
$SiNWs/TiO_2$	15.96	70.36	14.78	56,223	21.59
$C@SiNWs/TiO_2$	18.13	79.33	47.07	23,907	7.39

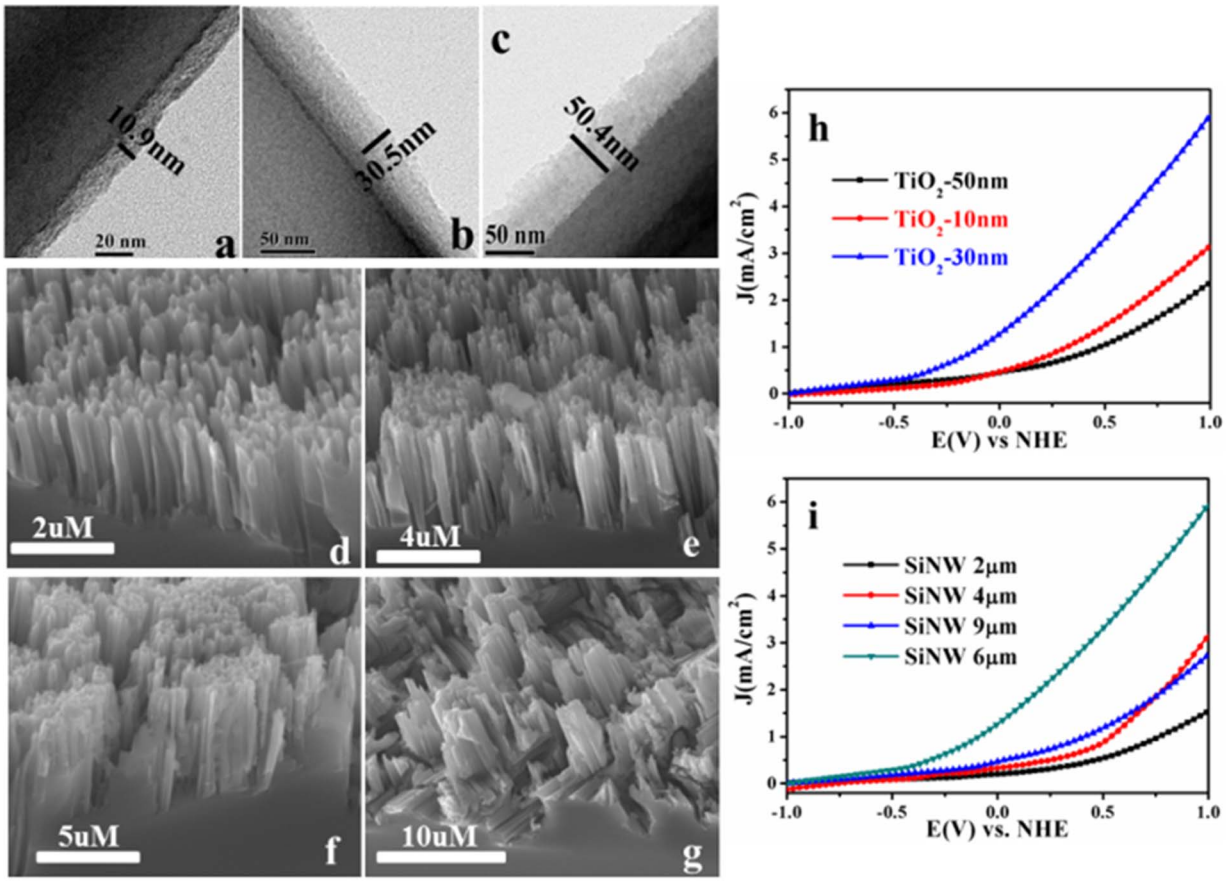

Figure 6 | TEM images of different thicknesses of TiO_2 on 6 μm long SiNWs (a–c) and their corresponding J-E curves under simulated illumination conditions (h). SEM images of different lengths of SiNWs with 30 nm TiO_2 thickness (d–g) and their corresponding J-E curves under simulated illumination conditions (i).

photocurrent densities as shown in Figure 6(h). The photocurrent density is highest for 30 ± 1 nm thick TiO_2 shell. In the case of less thick TiO_2 shell i.e. 10 ± 1 nm, the possible reason for decreased photocurrent density could be that the thickness is insufficient to separate the electron-hole pairs generated in TiO_2 and generated electrons to recombine with the holes generated in the silicon. Whereas in case of thicker TiO_2 shell i.e. 50 ± 1 nm, TiO_2 is completely covering the top surface of the SiNWs substrate, which will reduce the percolation of the electrolytes into the roots of the SiNWs and decreases the effective surface area resulting in lower photocurrent densities. Geometries, distribution density and length of SiNWs significantly affect their optical properties. In order to extract optimum efficiency, the length of SiNWs is systematically varied by controlling the etching time followed by evaluation for PEC performance. Accordingly, SEM images of C@SiNWs/TiO_2 core-shell heterostructures with varying lengths of SiNWs are given in the Figure 6 (d–g). Nanowires with approximate length of 2, 4, 6 and 9 μm are prepared by etching Si wafer for 10, 20, 30 and 60 min respectively. PEC measurements for these photoelectrode nanoarrays with SiNWs of varying length have been used to assess the effect of surface area on the photocurrent density by keeping the surface passivation parameters and TiO_2 thickness constant. For example, Figure 6(i) shows the J-E curves for photo anodes of different lengths of the SiNWs with TiO_2 shell of 30 nm in each case. By increasing the length of the SiNWs, the photocurrent densities are increased till 6 μm length of the nanowires. Further increase in the length of the SiNWs results in decreased photocurrent density. Possible reasons could be decreased distribution density of nanowires on Si substrate while chemical etching as prolonged etching could generate taller nanowires although simultaneous cross sectional etching also can lead to the removal of some of the SiNWs from silicon substrates. Subsequently the quantity of SiNWs exposed to the electrolytes can also get decreased ultimately to effect diminished photocurrent density. In addition, the transient photocurrent (J–t) test of the passivated and unpassivated heterostructured material carried out under intermittent light illumination and constant external bias (0.6 V vs. NHE) gives further confirmation. The chronoamperometric studies of the passivated and unpassivated samples shown in Figure 7(a) confirm the expected increase in photocurrent density of the passivated nanoarrays over that of the unpassivated nanoarrays. Increased photo current density in light for surface passivated photo electrode over the unpassivated one is due to decrease in recombination of electron-holes and increased interfacial charge transfer rate between silicon and TiO_2 layers. Under the same simulated illumination conditions, the photon conversion efficiencies (η) of the passivated and non passivated photo electrodes are calculated with the following equation[35].

$$\eta(\%) = J\left(\frac{mA}{cm2}\right)(1.23 - [|Voc - Vapp|]) * 100 \Big/ \text{Ptotal}\left(\frac{\text{mW}}{\text{cm2}}\right) \quad (2)$$

Where J is the photocurrent density under an applied bias potential V_{app}, V_{oc} is the open circuit potential (0.5 V vs. NHE), P_{total} is the incident light intensity (100 mW/cm^2) of the solar simulator as measured by a calibrated Si reference cell. As shown in Figure 7(b), the maximum photo conversion efficiencies for C@SiNW/TiO_2 and SiNW/TiO_2 are 1.17% (at 0.24 V vs.NHE), and 0.42% (0.38 V vs.NHE) respectively. Interestingly, these are some of the highest efficiency values reported so far in case of Si/TiO_2 core-shell structures. In comparison, wet etched SiNWs coated with TiO_2 shell by

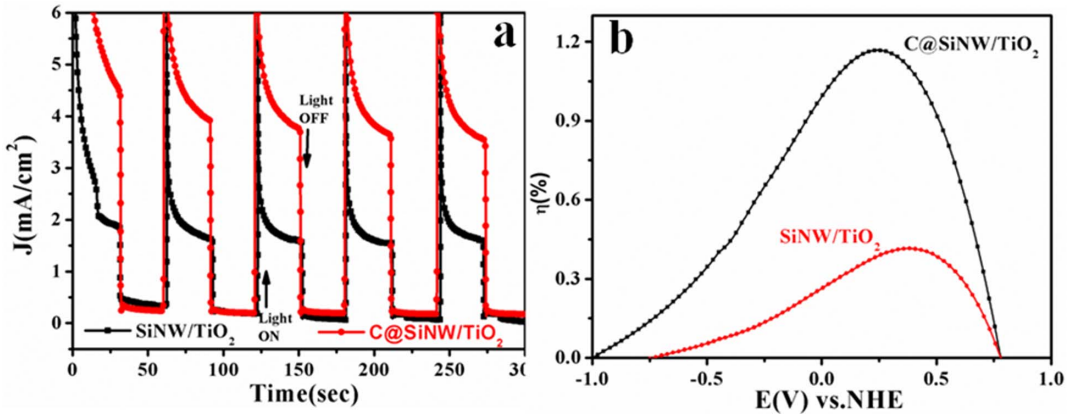

Figure 7 | (a) Chronoampererometric graphs with light off and on conditions of C@SiNWs/TiO_2 and SiNWs/TiO_2 nanowires and (b) Photo conversion efficiencies of the samples as a function of measured potentials w.r.t NHE.

ALD have shown a maximum photo electrochemical efficiency of only 0.42%[29]. This efficiency has been shown to increase up to 2.1% by 600 cycle SPCVD growth of 3D nanorods of TiO_2 on SiNWs. However, prior to applying the SiNW/TiO_2 NR architecture to PEC system, an additional layer of anatase TiO_2 polycrystalline thin film has been deposited by ALD (250 cycles) and all the photocurrent enhancement has been attributed to the TiO_2 NRs. Our results of 2.78 times higher efficiency for SiNW/TiO_2 core-shell structures with low cost organic/inorganic materials are far superior to all similar results recently reported in literature[29].

An efficient strategy is designed to passivate surface of MacEtch SiNWs in order to reduce defect site and enhance interfacial charge transfer between core (SiNWs) and shell (TiO_2) of a nano heterostructure photoelectrode enabling a remarkable improvement in performance. Organic surface reaction (photochemical alkylation) carried out with 1-octene on SiNW surface (H-terminated) followed by annealing creates a unique carbon passivation layer on SiNW surface. Photo electrochemical measurements show that such sandwich carbon layer between SiNW and TiO_2 increase photo electrochemical efficiency for water splitting reaction up to 1.17%, which is 2.78 times higher than that on unpassivated and previous such type of core-shell structures. Simplicity and efficiency of this approach to prepare surface passivated C@SiNW/TiO_2 nanoarrays with higher photo electrochemical efficiency will certainly open the door to facilitate many important applications in PEC and photovoltaic devices.

Methods

Materials and methods. All cleaning (H_2O_2, 30%; H_2SO_4, 96%) and etching (HF) reagents were of VLSI grade and supplied by Merck. All chemicals were of reagent grade or higher (purity > 99%) and were used as-received unless otherwise specified. Acetone, Isopropanol, nitric acid (HNO_3), hydrochloric acid (HCl), silver nitrate ($AgNO_3$), Titanium tetra tertbutoxide and 1-Octene were obtained from Aldrich.

Synthesis of SiNWs. A 1 × 1 cm^2 piece of phosphorous-doped, Si (100) wafer (1–5 Ω cm, Wafer net Inc.) was cleaned sequentially in acetone, Isopropanol and deionized (D.I.) water by ultrasonication for 5 min each. The Si wafer was then treated in boiling piranha solution (80°C) *i.e.* 98% H_2SO_4 : 30% H_2O_2 (3 : 1 in volume) for 20 min, followed by copious rinsing with D.I. water and finally dried under an Argon flow. The as-prepared Si wafer was then placed in a polytetrafluoroethylene (PTFE) vessel containing 4.6 M HF and 0.04 M $AgNO_3$ (1 : 1 in volume) and treated at 55°C for 30 min. After 30 minutes it was removed from the reaction solution, rinsed gently with D.I. water and then kept in a mixture of HNO_3 : HCl : H_2O (1 : 1 : 1 in volume) to remove the electroplated Ag. The as-prepared SiNW arrays were then treated in 5% HF solution for 1 min, rinsed with water, immediately dried in an Argon flow and used for the alkylation reaction. Length of SiNWs was optimized by systematically varying the etching time.

Surface passivation of SiNWs. Surface passivation of SiNWs was carried out by photochemical alkylation. In brief, H-terminated SiNWs were kept in a quartz cuvette filled with neat, degassed 1-octene solution and exposed to UV light for 6 hours. After the completion of reaction these alkylated SiNWs were subsequently washed with toluene and dichloromethane twice to remove any adsorbed 1-octene molecules on SiNWs surface. The alkylated SiNW arrays were immediately transferred into the furnace and annealed at 500°C in argon atmosphere for two hours.

Synthesis of surface passivated silicon-TiO_2 core-shell nanowires. The TiO_2 shell was formed on surface passivated silicon nanowires by dip coating of the titanium sol solution prepared by adding water (100 mM) and HNO_3 (1 drop) in Isopropanol solution drop wise to the solution of the Titanium tetra tertbutoxide (6.5 mM) in isopropanol under vigorous stirring and stirring was continued for the 12 hours. After that, the surface passivated SiNWs were dip coated for 25 cycles in the sol solution and annealed at 450°C for one hour in an argon atmosphere. The thickness of the TiO_2 shell on SiNWs was controlled by optimizing dipping cycles in the sol solution.

Characterization. Surface morphology of the material was examined by using a Quanta 200 3D, FEI scanning electron microscope (SEM). Transmission electron microscope (TEM) images were taken by using an FEI Technai300 keV microscope. X-Ray diffraction (XRD) studies were carried out on a Phillips PW 1830 instrument operating at 40 kV and a current of 30 mA with Cu Kα radiation. The reflectance spectra of the samples were measured by using Jasco UV–Vis spectrophotometer (V570 UV–VIS–NIR). FT-IR spectra of the samples were taken by using GX_Perkin Elmer (PSE) instrument with a resolution of 4 cm−1. X-ray photoelectron spectroscopy. X-ray photoelectron (XPS, Prevac) studies were done at 10-10 mbar pressure.

Photo electrochemical water splitting experiments. PEC characterizations were performed in a 1 M KOH electrolyte using a typical three-electrode electrochemical cell configuration by using a potentiostat (Biologic, SP-300). Surface passivated silicon/TiO_2 core-shell nanowires or nonpassivated silicon/TiO_2 core-shell nanowires (for comparison) were used as the working electrode; Pt foil served as the counter electrode; and Mercury/Mercury oxide (Hg/HgO) was used as the reference electrode. A 300 W Xe lamp (Science Tech) was coupled with a diffuser for uniform illumination intensity (samples typically 0.25–0.5 cm^2) and an AM 1.5 filter (Science Tech) for simulated sunlight. The illumination intensity was measured with a calibrated Si photodiode. Before measurement, the solar intensity was calibrated with a reference silicon solar cell and a read-out meter for solar simulator irradiance and an overall broad band illumination intensity of 100 mW/cm^2 was utilized. During PEC measurement, the electrolyte was degassed by Ar purging to remove the dissolved oxygen. IPCE for all the samples was investigated using a Quantum Efficiency Setup (Newport Corporation) under 1.0 V vs. NHE applied bias with 1 M aqueous KOH electrolyte by using three electrode assemblies. Photoelectrodes were used as the working electrode, Pt foil as counter electrode and Hg/HgO electrode as reference electrode.

1. Kamat, P. V. Meeting the clean energy demand: nanostructure architectures for solar energy conversion. *J. Phy. Chem. C.* **111**, 2834–2860 (2007).
2. Dresselhaus, M. S. & Thomas, I. L. Alternative energy technologies. *Nature.* **414**, 332–337 (2001).
3. Bard, A. J. & Fox, M. A. Artificial photosynthesis: solar Splitting of water to hydrogen and oxygen. *Acc. Chem. Res.* **28**, 141–145 (1995).
4. Grätzel, M. Photo electrochemical cells. *Nature* **414**, 338–344 (2001).
5. Walter, M. G. *et al.* Solar water splitting cells. *Chem. Rev.* **110**, 6446–6473 (2010).
6. Hochbaum, A. I. & Yang, P. Semiconductor nanowires for energy conversion. *Chem. Rev.* **110**, 527–546 (2010).
7. Yang, X. *et al.* Nitrogen-doped ZnO nanowire arrays for photo electrochemical water splitting. *Nano Lett.* **9**, 2331–2336 (2009).
8. Shankar, K. *et al.* Recent advances in the use of TiO_2 nanotube and nanowire arrays for oxidative photo electrochemistry. *J.Phy.Chem C* **113**, 6327–6359 (2009).

9. Wang, G. *et al.* Hydrogen-treated TiO_2 nanowire arrays for photo electrochemical water splitting. *Nano Lett.* **11**, 3026–3033 (2011).
10. Peng, K. Q. & Lee, S. T. Silicon nanowires for photovoltaic solar energy conversion. *Adv. Mater* **23**, 198–215 (2011).
11. Sivula, K., Le Formal, F. & Grätzel, M. Solar water splitting: progress using hematite (α-Fe_2O_3) photoelectrodes. *ChemSusChem.* **4**, 432–449 (2011).
12. Fujishima, A. & Honda, K. Electrochemical photolysis of water at a semiconductor electrode. *Nature* **238**, 37–38 (1972).
13. Li, Y. & Zhang, J. Z. Hydrogen generation from photo electrochemical water splitting based on nanomaterials. *Laser & Photonics Reviews.* **4**, 517–528 (2010).
14. Qiu, Y., Yan, K., Deng, H. & Yang, S. Secondary branching and nitrogen doping of ZnO nanotetrapods: building a highly active network for photo electrochemical water splitting. *Nano lett.* **12**, 407–413(2011).
15. Li, H. *et al.* Composition-graded $Zn_xCd_{1-x}Se$@ZnO core–shell nanowire array electrodes for photo electrochemical hydrogen generation. *J.Phy.Chem. C.* **116**, 3802–3807 (2012).
16. Sun, J., Liu, C. & Yang, P. Surfactant-free, large-scale, solution–liquid–solid growth of gallium phosphide nanowires and their use for visible-light-driven hydrogen production from water reduction. *J. Am. Chem. Soc.* **133**, 19306–19309 (2011).
17. Mohapatra, S. K., John, S. E., Banerjee, S. & Misra, M. Water photo oxidation by smooth and ultrathin α-Fe_2O_3 nanotube arrays. *Chem. Mater.* **21**, 3048–3055 (2009).
18. Sivula, K., Formal, F. L. & Grätzel, M. $WO_3-Fe_2O_3$ photo anodes for water splitting: a host scaffold, guest absorber approach. *Chem. Mater.* **21**, 2862–2867 (2009).
19. Bang, J. H. & Kamat, P. V. Solar cells by design: photo electrochemistry of TiO_2 nanorod arrays decorated with CdSe. *Adv. Func. Mater* **20**, 1970–1976 (2010).
20. Paracchino, A., Laporte, V., Sivula, K., Grätzel, M. & Thimsen, E. Highly active oxide photocathode for photo electrochemical water reduction. *Nat.Mater.* **10**, 456–461 (2011).
21. Zhang, R. *et al.* CdS/CdSe quantum dot shell decorated vertical ZnO nanowire arrays by spin-coating-based SILAR for photo electrochemical cells and quantum dot-sensitized solar cells. *ChemPhysChem* **13**, 1435–1439 (2012).
22. Li, Y. *et al.* vertically aligned Ta_3N_5 nanorod arrays for solar-driven photo electrochemical water splitting. *Adv. Mater.* **25**, 125–131 (2013).
23. Yuan, G. *et al.* Synthesis and photo electrochemical study of vertically aligned silicon nanowire arrays. *Angew.Chem. Int. Ed.* **48**, 9680–9684 (2009).
24. Kelzenberg, M. D. *et al.* Enhanced absorption and carrier collection in si wire arrays for photovoltaic applications. *Nat. Mater.* **9**, 239–244 (2010).
25. Santori, E. A. *et al.* Photo anodic behavior of vapour-liquid-solid–grown, lightly doped, crystalline Si micro wire arrays. *Energy Environ. Sci.* **5**, 6867–6871 (2012).
26. Oh, J., Deutsch, T. G., Yuan, H. C. & Branz, H. M. Nanoporous black silicon photocathode for H_2 production by photo electrochemical water splitting. *Energy Environ. Sci.* **4**, 1690–1694 (2011).
27. Peng, K. *et al.* Aligned single-crystalline Si nanowire arrays for photovoltaic applications. *Small.* **1**, 1062–1067 (2005).
28. Oh, I., Kye, J. & Hwang, S. Enhanced photo electrochemical hydrogen production from silicon nanowire array photocathode. *Nano lett.* **12**, 298–302 (2011).
29. Shi, J., Hara, Y., Sun, C., Anderson, M. A. & Wang, X. Three-dimensional high-density hierarchical nanowire architecture for high-performance photo electrochemical electrodes. *Nano lett.* **11**, 3413–3419 (2011).
30. Chen, Y. W. *et al.* Atomic layer-deposited tunnel oxide stabilizes silicon photoanodes for water oxidation. *Nat.Mater* **10**, 539–544 (2011).
31. Hwang, Y. J., Boukai, A. & Yang, P. High density n-Si/n-TiO_2 core/shell nanowire arrays with enhanced photo activity. *Nano lett.* **9**, 410–415 (2009).
32. Sun, K. *et al.* 3D branched nanowire heterojunction photoelectrodes for high-efficiency solar water splitting and H_2 generation. *Nanoscale.* **4**, 1515–1521 (2012).
33. Hwang, Y. J., Wu, C. H., Hahn, C., Jeong, H. E. & Yang, P. Si/InGaN core/shell hierarchical nanowire arrays and their photo electrochemical properties. *Nano lett.* **12**, 1678–1682 (2012).
34. Mayer, M. T., Du, C. & Wang, D. Hematite/Si nanowire dual-absorber system for photo electrochemical water splitting at low applied potentials. *J. Am. Chem. Soc.* **134**, 12406–12409 (2012).
35. Shankar, K. *et al.* Recent advances in the use of TiO_2 nanotube and nanowire arrays for oxidative photo electrochemistry. *J.Phy.Chem. C* **113**, 6327–6359 (2009).
36. Yuan, G. *et al.* Understanding the origin of the low performance of chemically grown silicon nanowires for solar energy conversion. *Angew. Chem., Int. Ed.* **50**, 2334–2338 (2011).
37. Cicero, R. L., Linford, M. R. & Chidsey, C. E. Photo reactivity of unsaturated compounds with hydrogen-terminated silicon (111). *Langmuir* **16**, 5688–5695 (2000).
38. Formal, F. L. *et al.* Passivating surface states on water splitting hematite photo anodes with alumina over layers. *Chem. Sci.* **2**, 737–743 (2011).

Acknowledgments

RRD acknowledges research fellowship from CSIR. Authors acknowledge Dr.Sarika Phadke for her assistance in IPCE measurements. This work was supported by the Council of Scientific and Industrial Research (CSIR), India through TAPSUN program.

Author contributions

R.R.D. has done the synthesis, characterization, Photo electrochemical and impedance measurements. R.R.D. has taken the help of J.D. in doing Mott-Schottky analysis and fitting of the impedance circuits. V.K.P. and M.V.S. discussed the technical contexts and made important suggestions. M.V.S. conceived the main idea and wrote whole manuscript. All authors reviewed the manuscript.

Additional information

Supplementary information accompanies this paper at http://www.nature.com/scientificreports

Competing financial interests: The authors declare no competing financial interests.

How to cite this article: Devarapalli, R.R., Debgupta, J., Pillai, V.K. & Shelke, M.V. C@SiNW/TiO_2 Core-Shell Nanoarrays with Sandwiched Carbon Passivation Layer as High Efficiency Photoelectrode for Water Splitting. *Sci. Rep.* **4**, 4897; DOI:10.1038/srep04897 (2014).